Nanostructures

DOI: 10.1002/anie.200605136

Iron–Gold Barcode Nanowires**

Ju Hun Lee, Jun Hua Wu, Hong Ling Liu, Ji Ung Cho, Moon Kyu Cho, Boo Hyun An, Ji Hyun Min, Su Jung Noh, and Young Keun Kim**

Nanowires are a focus of research interests as one-dimensional nanosystems and promise exciting applications in nanotechnology, ranging from nanoelectronic devices to cell separation and magnetic labeling in biomedicine.[1–5] A variety of methods have been devised to prepare them from magnetic,[6] semiconductor,[7] inorganic,[8] organic,[9] polymer,[10] metallic,[11] and dielectric materials[12] to provide nanowires with novel optical, electrical, catalytic, and magnetic properties. Multilayered or barcode arrangements of nanowires which incorporate different material components are a special case as a result of their spatial arraying, multiple functionalities, and enhanced properties in comparison to those of their single-component counterparts.[13–15] For instance, Co–Cu barcode nanowires were explored for their high magnetoresistance compared to that of the well-studied thin films,[16,17] while the coding of magnetic and optical properties in a single wire was targeted for the separation, detection, and transport of cells.[18]

Interested in the transport properties and potential applications of nanowires in nanodevices and biomedicine, we have investigated magnetic nanowires by electrodeposition.[19] For biomedical purposes, however, two issues have to be addressed for the implementation of such nanowires, namely surface modification and biocompatibility.[20] In this respect, the synthesis of iron–gold (Fe–Au) nanowires is appealing not only in terms of magnetic properties but also with respect to biological compatibility. On one hand, iron is favored as it is unique in the field of magnetic materials owing to its high magnetization and physicochemical potentiality. It can be easily converted into oxides, which have been thoroughly studied in the form of magnetic nanoparticles in the biomedical field for their magnetic properties and exceptional biocompatibility.[21] On the other hand, gold is a well-established material that displays attractive optical properties, biological compatibility, catalytic activity, and excellent surface effects.[22,23] Thus, it was anticipated that the integration of these two materials into a one-dimensional barcode arrangement on the nanoscale would produce a new nanostructured material that retains the optical and magnetic properties of the respective components, offering synergistically enhanced performance and functionalities which go beyond those of the individual components. Herein, we report the synthesis and characterization of such a kind of multifunctional magnetic–optical Fe–Au barcode nanostructures, that is, nanowires consisting of alternative Fe magnetic and Au optical segments.

The Fe–Au barcode nanowires were constructed using anodic alumina oxide (AAO) templates by pulse electrodeposition[19a] thus forming iron and gold segments alternatively in a single bath under desired pulse current densities (e.g. $10\,mA\,cm^{-2}$ and $0.5\,mA\,cm^{-2}$) with regulated pulse durations to control the respective segmental lengths (see Experimental Section). The selection of a current density to electrodeposit Fe or Au was based on the evaluation of the composition versus current density profile (Figure 1a), which was acquired from the analysis of the samples each obtained at a given constant current density, by inductively coupled

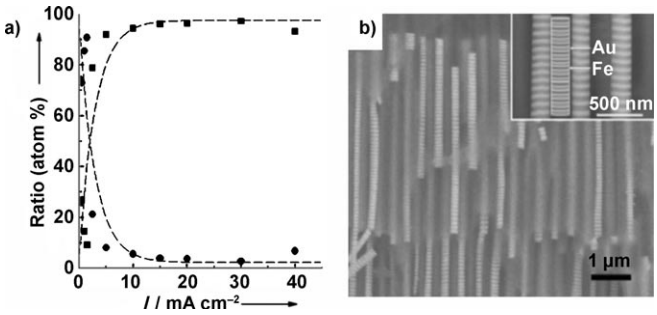

Figure 1. a) Composition versus current density profile of the nanowire samples each obtained at a given continuous current density (Fe ■; Au ●; the dashed lines are shown as a visual guide). b) FE-SEM image of the Fe–Au barcode nanostructures in AAO. The nanostructures were made up of alternative black and white parts, corresponding to Au and Fe layers. The inset shows an enlarged section of the image, with a schematic inserted between the first two nanowires to show the iron and gold layers.

[*] Prof. Dr. J. H. Wu
Research Institute of Engineering and Technology
Korea University
Seoul 136-713 (South Korea)
Fax: (+82) 2-928-3584
E-mail: wujh@korea.ac.kr
J. H. Lee, J. U. Cho, M. K. Cho, B. H. An, J. H. Min, S. J. Noh, Prof. Dr. Y. K. Kim
Department of Materials Science and Engineering
Korea University
Seoul 136-713 (South Korea)
Fax: (+82) 2-928-3584
E-mail: ykim97@korea.ac.kr
Dr. H. L. Liu
Institute for Nano Science
Korea University
Seoul 136-713 (South Korea)

[**] This work was supported by the Korea Science and Engineering Foundation grants M10633000049-06O3300-04910 (Pioneer Program) and M10500000105-05J0000-10510 (National Research Laboratory Program), the Korea Research Foundation grants KRF-2005-210-D00023 and KRF-2004-005-D00057, and the Korea Health 21 R&D Project grant A050750. We thank J. S. Ju and Y. S. Yoo for TEM measurements at Sungkyunkwan University.

plasma atomic emission spectrophotometer (ICP-AES). According to the data, the iron or gold composition in the electrodeposited nanowires changes rapidly with the current density and indicates no formation of an alloy between the two elements under our deposition conditions, as expected from their binary phase diagram.[24] Hence, a single-component nanowire may be acquired by using a current above 10 mA cm^{-2} for Fe and below 2 mA cm^{-2} for Au.

The formation of the barcode nanowires embedded in the AAO nanoporous array was demonstrated by field-emission scanning electron microscopy (FE-SEM; sample prepared under pulse deposition of 10 mA cm^{-2} for Fe and 0.5 mA cm^{-2} for Au; Figure 1b). The nanowires are composed of two alternative segments that represent the Fe and Au components, respectively, as seen in the inset, which shows an enlarged image of some barcode nanowires and a schematic arrangement of alterative Fe and Au segments in a single nanowire. This finding was substantiated by transmission electron microscopy (TEM) studies of the nanowires after removal of the template (Figure 2). The bright-field low-

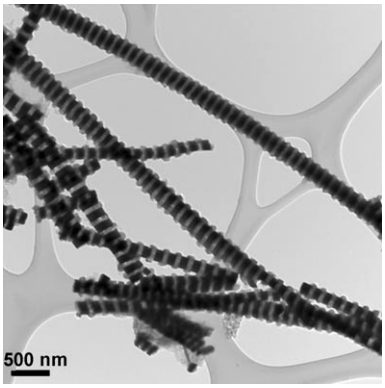

Figure 2. Bright-field TEM image of freestanding Fe–Au barcode nanowires, showing well-separated, alternate white and black parts that correspond to Fe and Au layers (bamboo-like nanostructures).

magnification image shows well-separated, bamboo-like nanostructures for the freestanding Fe–Au barcode nanowires. The contrast between the black and bright segments is distinct, and the respective compositions were identified by means of TEM elemental line scans and mapping (see below).

The crystal structure of the Fe–Au barcode nanowires in AAO was characterized by X-ray powder diffraction (XRD). Figure 3a shows the XRD profile for the sample prepared under a pulse deposition of 10 mA cm^{-2} for Fe and 0.5 mA cm^{-2} for Au in comparison with the standard diffraction peaks (in bars) of the corresponding constituent materials (JCPDS nos. 87-0721 and 04-0784; Figure 3b, c). The peaks at 38.14°, 44.36°, 64.58°, and 77.44° may be assigned to Au(111), (200), (220), and (311), while those at 44.36° and 64.58° are assigned to Fe(110) and (200). As a result of the superimposition of the peaks of Fe(110)/Au(200) and Fe-(200)/Au(220), the presence of elemental iron was derived directly from the selected-area electron-diffraction (SAED) pattern (Figure 3d), which was taken from the Fe segment determined by the elemental line scan and mapping shown in

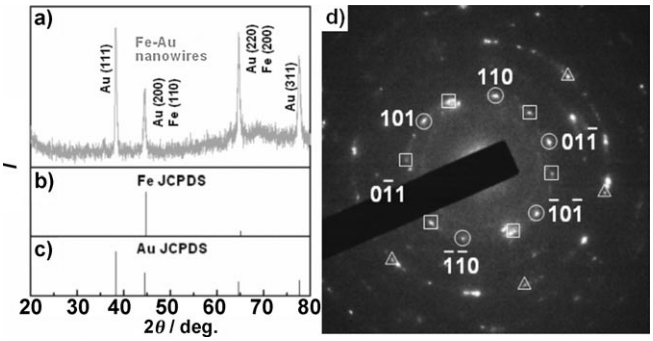

Figure 3. a) XRD pattern for the Fe–Au barcode nanowire array in AAO compared to the standard JCPDS data for b) Fe and c) Au. d) SAED pattern taken from one Fe segmental region. See text for details.

Figure 4. In the SAED pattern, multiple single-crystal diffraction patterns are recognizable and are labeled with circles for one set of Fe(110) and squares for another (the triangles signify the second-order diffraction spots corresponding to the set represented by the circles). This leads to the assignment of the spots to elemental iron, which is confirmed by the absence of Au(111) in the pattern. The analysis is consistent with the outcome of the SAED pattern obtained from nanowires deposited at a continuous current density of 10 mA cm^{-2}, which confirms the presence of iron in the elemental state. Furthermore, average crystalline domain sizes in the barcode nanowires can be estimated as approximately 26.1 nm for the Fe segments and about 24.0 nm for the Au segments from the full width at half-maximum in terms of the Scherrer equation, if the broadening of the peaks in the XRD patterns is primarily attributed to the finite size of the nanocrystals.[25] We note that there is a weak peak at approximately 35.5° that may be associated to Fe_3O_4(311) and/or Fe_2O_3(110) from the oxidation of the Fe surface.

Figure 4 shows the TEM image and the corresponding elemental mapping of an individual Fe–Au barcode nanowire after dissolving the template (sample prepared under pulse electrodeposition of 30 mA cm^{-2} for Fe and 0.5 mA cm^{-2} for Au). From the line scans, it is clear that the nanowire consists of alternative Fe and Au segments, thus confirming the results observed in Figure 1b and Figure 2. The homogeneity of the elemental distribution in the Fe and Au segments is revealed in the elemental mapping shown in Figure 4b, c.

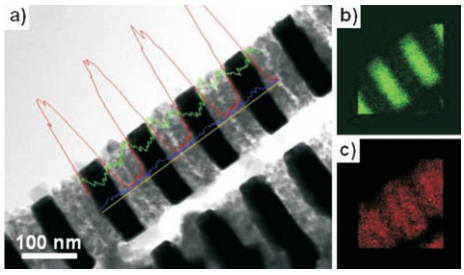

Figure 4. TEM analysis of a freestanding Fe–Au barcode nanowire. a) Elemental line scanning of Fe and Au composition along the nanowire (Au red, Fe green). b) Elemental mapping of Au. c) Elemental mapping of Fe.

The tailoring of the nanostructure of the Fe–Au nanowires was achieved by regulating the pulse durations. Figure 5 presents two examples of various Fe and Au segmental lengths, prepared by different pulse durations under the current densities of 10 mA cm^{-2} for Fe and 0.5 mA cm^{-2} for Au. In one case (Figure 5a), the Fe and Au segments are 62 nm and 60 nm (i.e. the segmental length ratio is near one), whereas in the other case (Figure 5b), the Fe and Au segments are 55 nm and 100 nm (i.e. the segmental length ratio is about 0.5). The change in the nanostructure of the barcode is reflected in its properties, as discussed below with respect to magnetism.

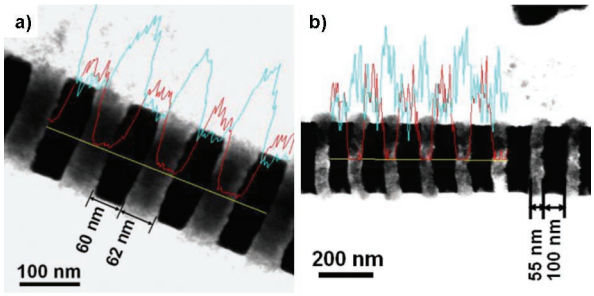

Figure 5. TEM images of freestanding Fe–Au barcode nanowires with different segmental lengths, with TEM elemental line scanning of Fe and Au composition (Au red, Fe blue) along the nanowires through energy-dispersive X-ray analysis (EDAX). a) Segmental length ratio of approximately 1. b) Segmental length ratio of approximately 0.5.

The magnetic properties of Fe–Au barcode nanowires of different segmental lengths were studied by using a vibrating sample magnetometer (VSM) at room temperature. The results of the Fe–Au barcode arrays in AAO shown in Figure 5a,b are given in Figure 6a,b, with the external magnetic field applied parallel and perpendicular to the nanowire axis, respectively. Both Fe–Au barcode arrays in AAO have their easy axis parallel to the nanowire axis and show soft ferromagnetic properties. For the array with a segmental length ratio of near unity, the coercivities parallel and perpendicular to the wires are 58 Oe and 28 Oe, respectively, whereas for the array with a segmental length ratio around 0.5, the coercivities are 42 Oe and 36 Oe, respectively. Moreover, the magnetic remanence is almost zero in both cases. For comparison, Figure 6c shows the data obtained for the Fe nanowire array in AAO deposited at a continuous current density of 10 mA cm^{-2}. The hysteresis curves are almost identical in both the parallel and perpendicular directions with coercivities of 300 Oe and 340 Oe, respectively, and the weak easy axis lies perpendicular to the nanowires. The result is in striking contrast to the commonly observed phenomena that the easy axis of Fe nanowire arrays lies parallel to the nanowire axis,[26] but showed up in a recent report of possible easy axis switching.[27] In fact, the determination of the easy axis of magnetic nanowire arrays is a complex issue that needs to be handled meticulously, as the measurements reflect the response of the ensemble and there is not an obvious method yet to extract the behavior of individual nanowires from the ensemble.[19a,28] Factors such as shape and mangnetocrystalline anisotropies, dipole–dipole interactions (e.g. lateral wire–wire interactions), and surface anisotropy, as well small dimensions have a dominant influence on the determination of the direction of the easy axis. In the present case, one other factor, namely the intersegmental interactions in the same nanowire and between different nanowires, needs also to be taken into consideration. Indeed, the switch in the easy axis is detected in our Fe–Au barcode nanosystem when the individual layer thicknesses were about 110 nm for the Fe layer and around 30 nm for the Au layer. Finally, the saturation magnetization of the Fe part, estimated to be approximately 230 emu g^{-1}, a value that lies quite near to that of bulk Fe but is much larger than that of iron oxides, further confirms the presence of elemental Fe in the nanowires.

The soft magnetic characteristic demonstrated in Figure 6 is useful, as it prevents the Fe–Au barcode nanowires from agglomeration which otherwise impedes the operation of individual nanowires. It was found that the Fe–Au barcode sample is easier to saturate compared to the pure Fe one, in which the susceptibility increases more rapidly, as observed in the case of gold-coated magnetic nanoparticles that behave superparamagnetically at room temperature.[29] This behavior has a direct impact on applications in such areas as biomedicine, where a larger susceptibility of the magnetic specimens boosts the performance of operation.[30] In addition, the behavior of magnetic response is described well by fitting the hysteresis curves satisfactorily to the Brillouin function or modified magnetization process, thus affording a basis for a deep understanding of the magnetic performance of the barcode nanowires.[31]

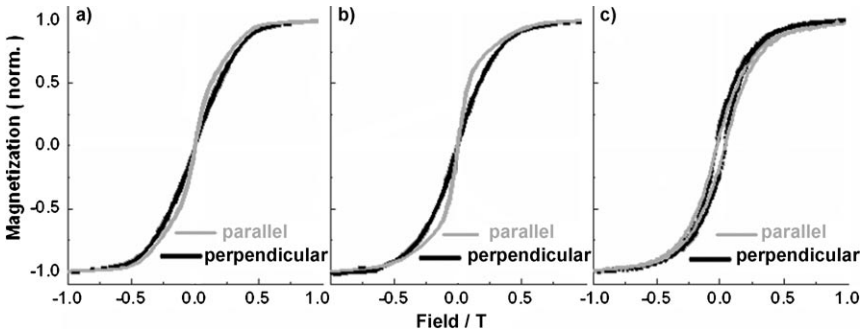

Figure 6. Hysteresis curves measured at room temperature for the Fe–Au barcode nanowire arrays in AAO as shown in Figure 5, compared to a pure Fe nanowire array. a) Segmental length ratio of approximately 1. b) Segmental length ratio of approximately 0.5. c) Fe nanowire array in AAO.

It is well known that nanostructured Au (e.g. nanoparticles and nanowires) exhibits an absorption band in the visible region owing to its surface plasmon, which is characteristic of the dimension, shape, and physicochemical environment surrounding the Au.[22,23,32] Figure 7a shows the UV/Vis absorption spectrum of the Fe–Au barcode nano-

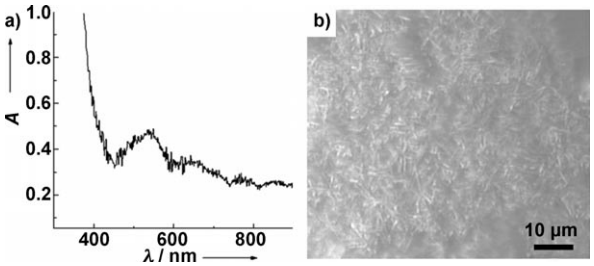

Figure 7. Optical measurements of the Fe–Au barcode nanowires. a) UV/Vis absorption spectrum of the Fe–Au barcode nanowires in ethanol after thiolation. b) Bright-field reflectance image.

wires prepared under pulse electrodeposition of 10 mA cm^{-2} for Fe and 0.5 mA cm^{-2} for Au and after thiolation to improve dispersion. The plasmon reveals the unique optical property of the barcode nanowires, and the absorption feature peaking at $\lambda \approx 530$ nm and ≈ 660 nm reflects the shaped Au segments[22,23,32] while the weak absorption located at $\lambda \approx 770$ nm and ≈ 850 nm could be attributed to the coupling between the Au segments. We note that the shifting and band shape is expected to depend on the Au segmental lengths. Although the direct contribution of the Fe segments to the spectrum is negligible, the close proximity of the nanomagnetic Fe segments to the Au segments may exert an influence on the optical properties of the nanowires. The bright-field reflectance image acquired using a Nikon Optiphot-100 (Figure 7b) in an optical microscopy study of the barcode nanowires shows the typical feature from gold.[15,22,23,32]

In summary, we have fabricated multifunctional magnetic–optical Fe–Au barcode nanowires by pulse electrodeposition in AAO. The thicknesses of individual layers were controlled by pulse durations. The characterization revealed that the resulting nanostructure displays the functions of both magnetic and optical constituents. The well-defined layered nanostructure of the Fe–Au barcode nanowires was confirmed through the structural analysis, TEM elemental line-scanning, and mapping which revealed well-separated, alternative arrangements of Fe and Au layers. Their magnetic properties revealed an easy axis that lies parallel to the nanowire axis and its possible switching by varying the segmental lengths, while the optical properties of the barcode nanowires were investigated by microscopic and spectroscopic measurements. The method presented herein should be easily extended to other systems (Co–Au, Ni–Au, etc.). Such a nanostructure reveals properties that are beyond those of the individual components, as a result of coupling of the optical sensing elements with the magnetic actuator, thereby presenting challenges in basic research and offering promise in applications. The Fe–Au barcode nanostructures are now the subject of studies concerning magnetic transport through a single nanowire and conjugation for cell separation, manipulation, and detection.

Experimental Section

The Fe–Au barcode nanowires were prepared in commercially available nanoporous anodic alumina oxide (AAO) membranes as templates (60 μm thick, 200 nm nominal pore diameter; Whatman Anodisk). Before electrodeposition, all the templates were coated with a layer of Au or Ag on one side to act as the working electrode, with a thin Pt sheet as the counter electrode. Electrodeposition was carried out in a single bath under a given cathodic pulse (e.g. 10 mA cm^{-2} and 0.5 mA cm^{-2}) generated by a Keithly 2400 power station for various durations to control the lengths of the individual barcodes. The bath consisted of iron(II) sulfate heptahydrate ($FeSO_4 \cdot 7H_2O$) and potassium dicyanoaurate ($KAu(CN)_2$) in deionized water, with the solution pH adjusted to pH 3.4–3.5 by using boric acid. The resultant magnetic–optical nanowires were freed from the templates through dissolution of the alumina in 1M NaOH solution, with an insignificant effect of etching on Fe.

The morphology and composition of the nanowires was evaluated by FE-SEM (Hitachi S-4300) with energy dispersive spectroscopy (EDS), ICP-AES (Jobin Yvon, 138 Ultrace), and TEM (JEOL 2010F) with the assistance of line scan, point probe, and elemental mapping in the EDX mode. The crystal structures of the nanowires were characterized by XRD ($Cu_{K\alpha}$, Bruker M18XCE) and SAED (JEOL 2010F). The magnetic properties of the iron–gold barcode nanowire arrays were analyzed by vibrating sample magnetometry (VSM, Lakeshore 7300). UV/Vis spectra were measured with an Agilent 8453E spectrophotometer and bright-field reflectance images were acquired using a Nikon Optiphot-100, both on samples dissolved in ethanol after thiolation.

Received: December 20, 2006
Revised: February 17, 2007
Published online: April 3, 2007

Keywords: electron microscopy · gold · iron · magnetic properties · nanostructures

[1] M. S. Gudiksen, L. J. Lauhon, J. F. Wang, D. C. Smith, C. M. Lieber, *Nature* **2002**, *415*, 617.
[2] a) Y. Cui, Q. Q. Wei, H. K. Park, C. M. Lieber, *Science* **2001**, *293*, 1289; b) F. Patolsky, B. P. Timko, G. Yu, Y. Fang, A. B. Greytak, G. Zheng, C. M. Lieber, *Science* **2006**, *313*, 1100; c) A. K. Salem, P. C. Searson, K. W. Leong, *Nat. Mater.* **2003**, *2*, 668.
[3] G. Che, B. Lakshmi, E. Fisher, C. Martin, *Nature* **1998**, *393*, 346.
[4] a) T. M. Whitney, J. S. Jiang, P. C. Searson, C. L. Chien, *Science* **1993**, *261*, 1316; b) T. Thurn-Albrecht, J. Schotter, G. A. Kastle, N. Emley, T. Shibauchi, L. Krusin-Elbaum, K. Guarini, C. T. Black, M. T. Tuominen, T. P. Russell, *Science* **2000**, *290*, 2126.
[5] a) J. I. Hahm, C. M. Lieber, *Nano Lett.* **2004**, *4*, 51; b) A. Hultgren, M. Tanase, E. J. Felton, K. Bhadriraju, A. K. Salem, C. S. Chen, and D. H. Reich, *Biotechnol. Prog.* **2005**, *21*, 509.
[6] a) A. Fert, L. Piraux, *J. Magn. Magn. Mater.* **1999**, 200, 338; b) P. S. Fodor, G. M. Tsoi, L. E. Wenger, *J. Appl. Phys.* **2002**, *91*, 8186; c) H. Zhu, S. Yang, G. Ni, D. Yu, Y. Du, *Scr. Mater.* **2001**, *44*, 2291.
[7] a) D. Bell, Y. Wu, C. J. Barrelet, S. Gradecak, J. Xiang, B. Timko, C. M. Lieber, *Microsc. Res. Tech.* **2004**, *64*, 373; b) D. Xu, D. Chen, Y. Xu, X. Shi, G. Guo, L. Gui, Y. Tang, *Pure Appl. Chem.* **2000**, *72*, 127; c) H. J. Fan, P. Werner, M. Zacharias, *Small* **2006**, *2*, 700.
[8] a) Y. Cai, S. K. Chan, I. K. Sou, Y. F. Chan, D. S. Su, N. Wang, *Adv. Mater.* **2006**, *18*, 109; b) A. R. Armstrong, G. Armstrong, J. Canales, P. G. Bruce, *Angew. Chem.* **2004**, *116*, 2336; *Angew. Chem. Int. Ed.* **2004**, *43*, 2286; c) H. K. Edwards, P. A. Salyer, M. J. Roe, G. S. Walker, P. D. Brown, D. H. Gregory, *Angew. Chem.* **2005**, *117*, 3621; *Angew. Chem. Int. Ed.* **2005**, *44*, 3555.
[9] a) A. Herland, P. Bjork, K. P. R. Nilsson, J. D. M. Olsson, P. Asberg, P. Konradsson, P. Hammarstrom, O. Inganas, *Adv. Mater.* **2005**, *17*, 1466; b) A. Mahler, M. Reches, M. Rechter, S. Cohen, E. Gazit, *Adv. Mater.* **2006**, *18*, 1365.

[10] a) T. Bjørnholm, T. Hassenkam, D. R. Greve, R. D. McCullough, M. Jayaraman, S. M. Savoy, C. E. Jones, J. T. McDevitt, *Adv. Mater.* **1999**, *11*, 1218; b) H. Cao, Z. Xu, H. Sang, D. Sheng, C. Tie, *Adv. Mater.* **2001**, *13*, 121; c) L. Zhang, C. F. Pan, J. Zhu, C. Wang, *Nanotechnology* **2005**, *16*, 2242; d) L. Feng, S. H. Li, H. J. Li, J. Zhai, Y. L. Song, L. Jiang, D. B. Zhu, *Angew. Chem.* **2002**, *114*, 1269; *Angew. Chem. Int. Ed.* **2002**, *41*, 1221; e) H. Liu, Y. Li, S. Xiao, H. Gan, T. Jiu, H. Li, L. Jiang, D. Zhu, D. Yu, B. Xiang, Y. Chen, *J. Am. Chem. Soc.* **2003**, *125*, 10794.

[11] a) G. E. Possin, *Rev. Sci. Instrum.* **1970**, *41*, 772; b) X.-R. Ye, Y. Lin, C. Wang, C. M. Wai, *Adv. Mater.* **2003**, *15*, 316; c) A. Fukuoka, Y. Sakamoto, T. Higuchi, N. Shimomura, M. Ichikawa, *J. Porous Mater.* **2006**, *13*, 231; d) A. J. Yin, J. Li, W. Jian, A. J. Bennett, J. M. Xu, *Appl. Phys. Lett.* **2001**, *79*, 1039.

[12] Y. Du, S. Han, W. Jin, C. Zhou, A. F. J. Levi, *Appl. Phys. Lett.* **2003**, *83*, 996.

[13] J.-r. Choi, S. J. Oh, H. Ju, J. Cheon, *Nano Lett.* **2005**, *5*. 2179.

[14] H.-P. Liang, Y.-G. Guo, J.-S. Hu, C.-F. Zhu, L.-J. Wan, C.-L. Bai, *Inorg. Chem.* **2005**, *44*, 3013.

[15] S. R. Nicewarner-Pena, R. G. Freeman, B. D. Reiss, L. He, D. J. Pena, I. D. Walton, R. Cromer, C. D. Keating, M. J. Natan, *Science* **2001**, *294*, 137.

[16] a) L. Piraux, J. M. George, J. F. Despres, C. Leroy, E. Ferain, R. Legras, K. Ounadjela, A. Fert, *Appl. Phys. Lett.* **1994**, *65*, 2484; b) A. Blondel, J. P. Meier, B. Boudin, J.-P. Ansermet, *Appl. Phys. Lett.* **1994**, *65*, 3019.

[17] a) H. Kano, K. Kagawa, A. Suzuki, A. Okabe, K. Hayashi, K. Aso, *Appl. Phys. Lett.* **1993**, *63*, 2839; b) W. H. Rippard, R. A. Buhrman, *Phys. Rev. Lett.* **2000**, *84*, 971.

[18] D. H. Reich, M. Tanase, A. Hultgen, L. A. Bauer, C. S. Chen, G. J. Meyer, *J. Appl. Phys.* **2003**, *93*, 7275.

[19] a) J. U. Cho, J. H. Min, S. P. Ko, J. Y. Soh, Y. K. Kim, J.-H. Wu, S. H. Choi, *J. Appl. Phys.* **2006**, *99*, 08C909; b) J. U. Cho, J.-H. Wu, J. H. Min, S. P. Ko, J. Y. Soh, Q. X. Liu, Y. K. Kim, *J. Magn. Magn. Mater.* **2006**, *303*, e281; c) J. H. Min, B. H. An, J. U. Cho, H. M. Ji, S. J. Noh, Y. K. Kim, H. L. Liu, J. H. Wu, *J. Appl. Phys.* **2006**, in press.

[20] a) A. K. Wanekaya, W. Chen, N. V. Myung, A. Mulchandani, *Electroanalysis* **2006**, *18*, 533; b) L. A. Bauer, N. S. Birenbaum, G. J. Meyer, *J. Mater. Chem.* **2004**, *14*, 517.

[21] a) A. K. Gupta, M. Gupta, *Biomaterials* **2005**, *26*, 3995; b) D. L. Huber, *Small* **2005**, *1*, 482; c) F. Walz, *J. Phys. Condens. Matter* **2002**, *14*, R285.

[22] a) M.-C. Daniel, D. Astruc, *Chem. Rev.* **2004**, *104*, 293; b) M. Hu, J. Chen, Z.-Y. Li, L. Au, G. V. Hartland, X. Li, M. Marqueze, Y. Xia, *Chem. Soc. Rev.* **2006**, *35*, 1084.

[23] a) B. D. Busbee, S. O. Obare, C. J. Murphy, *Adv. Mater.* **2003**, *15*, 414; b) Y.-Y. Yu, S.-S. Chang, C.-L. Lee, C. R. C. Wang, *J. Phys. Chem. B* **1997**, *101*, 6661; c) B. M. I. van der Zande, M. R. Bohmer, L. G. J. Fokkink, C. Schonenberger, *Langmuir* **2000**, *16*, 451; d) S. Link, M. B. Mohamed, M. A. El-Sayed, *J. Phys. Chem. B* **1999**, *103*, 3073.

[24] *Smithells Metals Reference Book* (Ed.: E. A. Brandes), Butterworths, Singapore, **1983**, pp. 11 – 74.

[25] B. D. Cullity, S. R. Stock, *Elements of X-ray Diffraction*, Prentice Hall, New Jersey, **2001**, pp. 167 – 171.

[26] a) S. Yang, H. Zhu, D. Yu, Z. Jin, S. Tang, Y. Du, *J. Magn. Magn. Mater.* **2000**, *222*, 97; b) X. Y. Zhang, G. H. Wen, Y. F. Chan, R. K. Zheng, X. X. Zhang, N. Wang, *Appl. Phys. Lett.* **2003**, *83*, 3341; c) Y. Peng, H.-L. Zhang, S.-L. Pan, H.-L. Li, *J. Appl. Phys.* **2000**, *87*, 7405.

[27] J. B. Shi, Y. J. Chen, Y. T. Lin, C. Wu, C. J. Chen, J. Y. Lin, *Jpn. J. Appl. Phys.* **2006**, *45*, 9075.

[28] L. Sun, Y. Hao, C.-L. Chien, P. C. Searson, *IBM J. Res. Dev.* **2005**, *49*, 79, and references therein.

[29] L. Y. Wang, J. Luo, Q. Fan, M. Suzuki, I. S. Suzuki, M. H. Engelhard, Y. H. Lin, N. Kim, J. Q. Wang, C. J. Zhong, *J. Phys. Chem. B* **2005**, *109*, 21593.

[30] Q. A. Pankhurst, J. Connolly, S. K. Jones, J. Dobson, *J. Phys. D* **2003**, *36*, R167.

[31] a) R. C. O'Handley, *Modern Magnetic Materials: Principles and Applications*, Wiley, New York, **2000**, p. 91; b) J. H. Wu, *Nanotechnology* **2002**, *13*, 720.

[32] P. Mulvaney, L. M. Liz-Marzan, M. Giersig, T. Ung, *J. Mater. Chem.* **2000**, *10*, 1259.

